Published in final edited form as:
J Phys Chem C Nanomater Interfaces. 2009 November 5; 113(44): 19021–19027. doi:10.1021/jp906394z.

NIR-responsive silica-coated $NaYbF_4$:Er/Tm/Ho upconversion fluorescent nanoparticles with tunable emission colors and their applications in immunolabeling and fluorescent imaging of cancer cells

Meng Wang[a], **Congcong Mi**[a], **Yixin Zhang**[a], **Jinling Liu**[a], **Feng Li**[a], **Chuanbin Mao**[b,*], and **Shukun Xu**[a,*]

[a]Department of Chemistry, Northeastern University, Shenyang, 110004, P. R. China

[b]Department of Chemistry & Biochemistry, University of Oklahoma. 620 Parrington Oval, Room 208, Norman, Oklahoma 73019, USA

Abstract

$NaYbF_4$: RE upconversion (UC) fluorescent nanoparticles (NPs) were synthesized with variable rare-earth dopants (RE= Er^{3+}, Tm^{3+}, or Ho^{3+}, or a combination of these ions), from rare-earth stearate precursors in a water-ethanol-oleic acid system by using a two-phase solvothermal method. The NPs were shown to emit visible light such as orange, yellow, green, cyan, blue or pink light in response to near infrared (NIR) irradiation, and their emission colors could be simply tuned by changing either the co-dopant concentration or dopant species. The UC NPs were well-dispersed and spherical with an average size of 15~35 nm. They emitted strong UC fluorescence under the 980 nm NIR excitation. The effects of solvothermal reaction time and temperature on nanoparticle size and phase structure as well as UC fluorescence intensity were systematically studied. Water dispersibility was achieved by forming a silica coat on the surface of the UC NPs. After animo-functionalization, the silica-coated UC NPs were chemically conjugated with the rabbit anti-CEA8 antibody and then used as fluorescent biolabels for the immunolabeling and imaging of HeLa cells. The NIR-responsive multicolor visible light emission of these UC NPs will enable potential applications in biolabeling and multiplexed analysis because NIR light can penetrate tissue as deep as several inches and is safe to human body.

1. Introduction

Research on fluorescent nanoparticles (NPs) has gained considerable attention due to their applications in multicolor imaging (1) and multiplexed analysis (2,3). The first use of red and green quantum dots (QD) as fluorescent labels for multicolor imaging of fixed mouse fibroblasts was reported in 1998 (4). Multicolor QDs-coded fluorescent microspheres also find applications as fluorescent label for the detection of biomolecules (5,6). The major advantage of these NPs is their ability to emit many colors which could be simultaneously detected, upon excitation by a single wavelength of light, thus simplifying the performance of multiplex analysis (7). The major drawback of the current fluorescent labels (such as QDs and organic dyes) excited by blue or ultraviolet (UV) radiation is that they can induce the autofluorescence from the biological molecules or tissues (8). It is perceived that the autofluorescence from biomolecules can be avoided if the fluorescent labels can be excited by near-infrared (NIR) or

*To whom correspondence should be addressed. Tel.: 86 24 83681343, xushukun46@126.com (S. K. Xu)
*To whom correspondence should be addressed. Tel: 1 405 325 4385, cbmao@ou.edu (C. B. Mao).

infrared (IR) light. Such NIR-responsive fluorescent labels will lead to a higher signal-to-noise ratio and thus improved performance in bioimaging and detection. In particular, NIR light is safe to human body and can penetrate tissue with a depth up to several inches. Thus, nanoparticles that can emit visible lights in response to the excitation by NIR light can have potential application in in vivo fluorescent imaging.

In recent years, upconversion (UC) NPs have attracted considerable interests owing to their unique optical properties (9-13). UC is an anti-Stokes process where a longer wavelength radiation, usually NIR or IR light, is converted to a shorter wavelength such as UV or visible (VIS) radiation via a two-photon or multi-photon mechanism (14). In comparison to the traditional fluorescent labels such as organic dyes and QDs, UC NPs can be excited by IR radiation with an excellent signal-to-noise ratio owing to the absence of autofluorescence and reduction of light scattering (5,16). In addition, UC NPs also have prominent advantages such as narrow emission peak, large Stokes shifts, good chemical/physical stability, and low toxicity (17). Thus, there is a high demand in the synthesis of multicolor high quality UC NPs that can be applied to biodetection. The actively studied UC NPs are rare-earth (RE) fluorides (18-20) and can be prepared by thermal decomposition (21-28), hydrothermal and solvothermal method(29-31), coprecipitation (20,32,33), or liquid-solid-solution (LSS) phase transfer and separation approach (34,35).

Here we report the use of a solid-liquid two-phase solvothermal method to synthesize $NaYbF_4$ UC fluorescent NPs doped with one or two RE ions (Er^{3+}, Tm^{3+}, or Ho^{3+}). The new fluorescent NPs can emit orange, yellow, green, cyan, blue, or pink light under a NIR irradiation (980 nm), depending on the dopant species and concentrations. The as-synthesized NPs have been characterized by TEM, powder XRD and luminescence spectroscopy. Water dispersibility has been achieved by the formation of a silica shell through typical Stöber-based surface modification. The effects of reaction time and temperature on size, phase and UC fluorescence intensity of the NPs are studied and discussed in detail. The $NaYbF_4$:Er/Tm/Ho UC NPs were linked to the rabbit anti-CEA8 antibody and then used as the fluorescent biolabels for the immunolabeling and imaging of live HeLa cells.

2. Experimental Section

2.1. Materials

Rare-earth oxides used in this work including ytterbium oxide (Yb_2O_3), erbium oxide (Er_2O_3), thulium oxide (Tm_2O_3), and holmium oxide (Ho_2O_3) were of 99.99% purity. Sodium fluoride (NaF), stearic acid ($C_{17}H_{35}COOH$), oleic acid ($C_{17}H_{33}COOH$), ammonia ($NH_3{\cdot}H_2O$), sodium hydroxide (NaOH), nitric acid (HNO_3), 3-aminopropyltrimethoxysilane (APTES) and tetraethyl orthosilicate (TEOS) were of analytical grade. All the chemicals above were purchased from Sinopharm Chemical Reagent Co., Ltd. (Shanghai, China). N-ethyl-N'-[3-(dimethylamino)propyl]carbodiimide hydrochloride (EDC), and N-hydroxysuccinimide (NHS) were purchased from Acros (USA). Primary antibody (Ab) rabbit anti-CEA8 and bovine serum albumin (BSA) were purchased from Biosynthesis Biotechnology Co. Ltd. (Beijing, China). HeLa cells were obtained from China Medical University. Triple-distilled water was used throughout the experiments.

2.2. Characterization

The size and morphology of as-prepared NPs were observed on a JEM-2100HR transmission electron microscope (TEM, JEOL Ltd., Japan), using an accelerating voltage 200 kV. X-ray diffraction (XRD) measurements were performed on a D/max 2500/PC diffractometer (JEOL Ltd., Japan) at a scanning rate of 8°/min, with graphite monochromatized Cu Kα radiation (λ=0.15406 nm). UC fluorescence spectra of the dried and powdered NPs were measured on

a LS-55 fluorescence spectrophotometer (Perkin Elmer Co., USA) attached with an external 980 nm laser (Beijing Hi-Tech Optoelectronic Co., China) instead of the internal excitation source. The maximum power of the laser was 1250 mW. Fourier transform infrared (FT-IR) spectra of the silica-coated NPs were measured on a spectrum One (B) spectrometer (Perkin Elmer Co., USA) by using KBr method.

2.3. Synthesis of rare-earth stearate precursors

To synthesize ytterbium stearate precursor, 1.9704 g (5 mmol) Yb_2O_3 was dissolved in nitric acid by heating to form the ytterbium nitrate. Solvent drying resulted in the formation of nitrate powder. In a 500 ml three-neck flask, the as-prepared powder and 8.5344 g (30 mmol) stearate acid were dissolved in 60 mL ethanol under vigorous stirring at 50 °C. Subsequently, after the temperature was increased to 78 °C, 1.1900 g NaOH (30 mmol) in 15 ml of water was added dropwise into the flask over a period of 30 min. The resultant mixture was refluxed at 78 °C for another 30 min. Precipitates from the reaction mixture were filtered, washed three times with water and once with ethanol. Ytterbium stearate precursor was obtained by drying the precipitates at 60 °C for 12 h. Other stearate precursors such as those of erbium, thulium and holmium were prepared in a similar manner employing Er_2O_3, Tm_2O_3 and Ho_2O_3, respectively.

2.4. Synthesis of rare-earth doped $NaYbF_4$ UC NPs

To synthesize $NaYb_{0.98}F_4:Er_{0.02}$ UC NPs, 10 ml water, 15 ml ethanol, and 5 ml oleic acid were mixed together under stirring to form a homogeneous solution, to which 1.0030 g (0.98 mmol) ytterbium stearate, 0.0204 g (0.02 mmol) erbium stearate and 0.2099 g (5 mmol) NaF were added. The mixture was stirred for about 15 min, transferred to a 50 ml autoclave, sealed, and solvothermally treated at 150 °C for 24 h. After the autoclave was cooled to room-temperature naturally, the precipitates were separated by centrifugation, washed with ethanol three times and then dried for 12 h. Other kinds of rare-earth doped $NaYbF_4$ NPs were synthesized in a similar manner by varying the amount of rare-earth stearate precursors.

2.5. Surface modification of rare-earth doped $NaYbF_4$ UC NPs

In a 250 ml flask, 20 mg of $NaYb_{0.98}F_4:RE_{0.02}$ UC NPs were dispersed in 60 ml 3-propanol by sonication and agitation for 40 min. 2.5 ml ammonia and 20 ml water were added to the flask and maintained at 35 °C under vigorous stirring. A solution containing 20 ml 3-propanol and 25 μl TEOS was added dropwise to the mixture over a period of 1 h and the reaction continued for another 3 h. The precipitates were separated by centrifugation, washed with ethanol three times, and then dried at 60 °C for 12 h to obtain silica-coated $NaYb_{0.98}F_4:RE_{0.02}$ UC NPs. The amino-functionalized $NaYb_{0.98}F_4:RE_{0.02}$ UC NPs were prepared as the same process by adding the solution containing 30 ml 3-propanol and 200 μl APTES slowly to the mixture followed by the addition of TEOS solution.

2.6. Preparation of rabbit anti-CEA8 antibody conjugated UC NPs

The NHS/EDC chemistry (36-38) was employed for the conjugation of amino-modified UC NPs with rabbit anti-CEA8 antibody (Ab). Typically, 100 μl of 0.1 mg/ml rabbit anti-CEA8 Ab solution in 10 mmol/l phosphate buffer solution (PBS) of pH 7.4, was mixed with 100 μl of 2.0 mg/ml amino-modified UC NPs solution in the same buffer. The mixture was activated by 50 μl of 0.2 mg/ml EDC and 25 μl of 0.2 mg/ml NHS for 10 min at room temperature, and the reaction was continued for 2 h at 37 °C in a reciprocating oscillator. The rabbit anti-CEA8 Ab conjugated UC NPs were purified by centrifugation, washed with PBS twice and dissolved in 2 ml PBS.

2.7. Cell culture, immunolabelling and fluorescent imaging

The HeLa cells were cultured (at 37 °C, 5% CO_2) on glass chamber slides in RPMI 1640 medium containing 10% fetal bovine serum and 1% penicillin/streptomycin overnight in a culture box (Heraeus BB16UV). The cells were gently washed three times with PBS and blocked in PBS containing 1% bovine serum albumin (BSA) for 20 min at 4 °C. Then, HeLa cells were incubated with rabbit anti-CEA8 Ab conjugated UC NPs at 4 °C for 1 h. The control experiment was conducted in the same manner except that the amino-modified UC NPs were used instead of the rabbit anti-CEA8 Ab conjugated UC NPs. Before imaging, the live cells were washed thoroughly with PBS to remove any unbound reagents. Cell imaging was performed on a Leica DMIL inverted fluorescence microscope equipped with a 980 nm NIR laser and a Nikon digital camera (Figure S1).

3. Results and Discussion

In this work, $NaYbF_4$:RE UC NPs with different rare-earth dopants were synthesized in a water-ethanol-oleic acid system by using rare-earth stearate as a precursor. Briefly, NaF was dissolved in water-ethanol-oleic acid system, which serves as the liquid phase. Rare-earth stearate owing to its insolubility in the water-ethanol-oleic acid system is dispersed into the solution as a solid phase. At an elevated temperature, the rare-earth stearate decomposes slowly, thus releasing RE^{3+} ions, which in turn reacted with Na^+ and F^- ions in the liquid phase. The efficiency of this two-phase reaction is much lower than that in homogeneous solution (39, 40), and therefore requires longer reaction time and high temperature. We found that the reaction time and temperature had great influence on the size, phase, and UC fluorescence intensity of $NaYb_{0.98}F_4$:$Er_{0.02}$ UC NPs.

3.1. Size characterization of $NaYb_{0.98}F_4$:$Er_{0.02}$ UC NPs

TEM images of $NaYb_{0.98}F_4$:$Er_{0.02}$ NPs synthesized at 150 °C for 2, 8, and 24 h are presented in Figure 1a, b and c, respectively. When the reaction time was maintained at 2 h, the NPs were spherical in shape with an average size of 15 nm (Figure 1a). On increasing the reaction time to 8 h, the NPs were still spherical and had a size of about 25 nm (Figure 1b). When the reaction time was further extended to 24 h, the size of the NPs was slightly increased to about 30 nm, and the shape of the NPs remained almost unchanged (Figure 1c). Similar observations have also been made when the reaction time was maintained constant and the reaction temperature was varied (Figure 1d, b, and e), with an average size of 15 nm, 30 nm, and 35 nm being observed at 100 °C, 150 °C and 200 °C, respectively. Thus it can be concluded that the reaction time and temperature plays an important role in controlling size of the $NaYb_{0.98}F_4$:$Er_{0.02}$ NPs.

3.2. Structural characterization of $NaYb_{0.98}F_4$:$Er_{0.02}$ UC NPs

$NaREF_4$ exists either in cubic α-phase (metastable high-temperature phase) or hexagonal β-phase (thermodynamically stable low-temperature phase) at ambient pressure (41). In most cases, cubic α-phase $NaREF_4$ can be obtained under mild conditions, such as short reaction time and low temperature, or even room temperature. However, hexagonal β-phase $NaREF_4$ can be obtained from α-$NaREF_4$ via a cubic-to-hexagonal phase transition process under relatively drastic conditions, such as long reaction time and high temperature (42). During the experiment, we found that the reaction time and temperature were two main influential factors in the phase transition of $NaYb_{0.98}F_4$:$Er_{0.02}$ NPs.

XRD patterns of $NaYb_{0.98}F_4$:$Er_{0.02}$ NPs synthesized at 150 °C after different reaction times (2, 8, and 24 h) are presented in Figure 2a. When the reaction time was maintained at 2 h, the XRD pattern matched well with that of cubic α-phase $NaYbF_4$ (JCPDS No. 77-2043) (Figure 2c). With the reaction time increased to 8 h, the intensities of peaks assigned to cubic α-phase are increased, and some new diffraction peaks which can be indexed to the hexagonal β-phase

$NaYbF_4$ (JCPDS No. 27-1427) are observed, indicating that the NPs synthesized at 150 °C for 8 h are composed of a major cubic α-phase and a minor hexagonal β-phase. The above phenomena can be attributed to the cubic-to-hexagonal phase transition process. When the reaction time is further extended to 24 h, the peaks belonging to the hexagonal β-phase are all significantly enhanced while those corresponding to the cubic α-phase are weakened. However, the NPs cannot be transformed from cubic α-phase to hexagonal β-phase completely with a reaction time of 24 h at 150 °C. The XRD patterns of $NaYb_{0.98}F_4:Er_{0.02}$ NPs synthesized for 8 h at different temperatures (100 °C, 150 °C and 200 °C) are shown in Figure 2b. Similarly, when the temperature is relatively low, *i.e.* 100 °C, only pure cubic α-phase NPs were obtained. As the temperature reaches 150 °C, a small quantity of hexagonal β-phase can be observed along with the cubic α-phase. At 200 °C, the quantity of hexagonal β-phase increases significantly, which indicates the enhancement of cubic-to-hexagonal phase transition process. These results clearly indicate that reaction time and temperature show tremendous influence on the phase structure of $NaYb_{0.98}F_4:Er_{0.02}$ NPs, and the process of cubic-to-hexagonal phase transition can be enhanced by employing appropriate reaction time and temperature. While pure cubic α-phase NPs can be prepared at a lower temperature (~100 °C) and a shorter reaction time (~2 h), both higher temperature and extended reaction time are required to form pure hexagonal β-phase NPs.

3.3. UC fluorescence properties of $NaYb_{0.98}F_4:Er_{0.02}$ UC NPs

Reaction time and temperature also had a noticeable impact on the UC fluorescence of the NPs. Figure 3 shows the UC fluorescence spectra of the $NaYb_{0.98}F_4:Er_{0.02}$ NPs synthesized at different reaction times (Figure 3a) and temperatures (Figure 3b). From the UC fluorescence spectra in Figure 3a, the NPs synthesized at 150 °C for 2 h and 4 h show nearly no fluorescence. Fluorescence intensity is increased when the reaction time was extended first to 8 h and then to 12 h. Furthermore, the fluorescence intensity was enhanced significantly when the reaction time was further prolonged to 24 h. A varying reaction temperature at a constant reaction time of 8 h had a similar effect on the UC fluorescence. A low fluorescence intensity is observed at 100 and 120 °C, while appreciable increasing intensity is observed as temperature is increased to 150, 180 and 200 °C, respectively.

From the XRD and fluorescence measurements it can thus be fairly concluded that the hexagonal β-phase $NaYb_{0.98}F_4:Er_{0.02}$ NPs show strong UC fluorescence while cubic α-phase NPs give almost no emission, and the intensity of fluorescence emission increases with the formation of hexagonal phase $NaYb_{0.98}F_4:Er_{0.02}$ NPs. Therefore, it is reasonable to postulate that the UC fluorescence intensity of $NaYb_{0.98}F_4:Er_{0.02}$ NPs is phase-dependent, which is in agreement with the reported case of other UC NPs (32,33).

The dependence of fluorescence intensity (green emission at 541 nm) on the reaction times (2~24 h) and temperatures (100~200 °C) is presented in Figure 3c. An increase in the fluorescence intensity is observed at prolonged reaction times and elevated temperatures, which is related to the cubic-to-hexagonal phase transition. Thus the jump of the fluorescence intensity can be an indicator of the cubic-to-hexagonal phase transition. At a reaction temperature of 100 °C, fluorescence intensity remains almost unchanged, indicating that there is no or only little occurrence of phase transition at the synthesis temperature of 100 °C and the hexagonal phase occurs only at a higher temperature. When the temperature is elevated, the fluorescence intensities begin to jump at prolonged reaction time. For instance, fluorescence intensity of the NPs synthesized at 120 °C begins to jump when the reaction time reached 4 h, indicating that the cubic-to-hexagonal phase transition took place at 4 h. Furthermore, the higher the synthesis temperature is, the earlier the jump phenomenon occurs, and the earlier the cubic-to-hexagonal phase transition occurs.

The concentration of dopant ions (Er^{3+} ion) also impacts the UC fluorescence intensity of $NaYbF_4$:Er NPs. Following a reported procedure, we calculated the integrated intensity as a sum of integrated area of the red and green peaks (23,24). Figure 4 shows UC intensity (sum of integrated peak area for peaks corresponding to the green and red emission) of $NaYbF_4$:Er NPs synthesized at different dopant concentrations. When the concentration of Er^{3+} is very low (1%), the fluorescence intensity is not very strong because there are not enough Er^{3+} ions acted as the luminescence centers for the UC emission. As the concentration of Er^{3+} is increased to 2%, the fluorescence intensity reaches the highest value. When Er^{3+} concentration is further increased, the fluorescence intensity decreases gradually, which is primarily ascribed to the cross-relaxation process of Er^{3+} ions (43). With the further increase of the concentration of Er^{3+} ions in the host ($NaYbF_4$) lattice, the distance between neighboring Er^{3+} ions becomes shorter, which can enhance the interaction of the neighboring Er^{3+} ions and intensify the cross-relaxation process of Er^{3+} ions, resulting in the concentration-dependent quenching.

3.4. Surface silica coating

The surfaces of the NPs prepared in a water-ethanol-oleic acid system are capped with a layer of oleic acid molecules, as confirmed from FT-IR spectrum shown in Figure 5a. The oleic acid exhibits a broad band at around 3419 cm^{-1}, corresponding to the stretching vibration of hydroxyl group. Two peaks associated with the asymmetric and symmetric stretching vibrations of the carboxylic group (COO^-) can be found at 1565 and 1458 cm^{-1} in the spectrum, respectively. In addition, two peaks at 2924 cm^{-1} and 2853 cm^{-1} are assigned to the asymmetric and symmetric stretching vibrations of methylene group which exists in the long alkyl chain of oleic acid molecule. The capped oleic acid is difficult to remove upon washing, which in turn retards the water dispersibility of the NPs. After a typical Stöber-based surface modification, the NPs are modified to have hydrophilic surfaces by coating a layer of silica, and can thus be easily dispersed in water to form a colloidal solution. TEM image of silica-coated NPs is displayed in Figure 6a. The NPs are well-dispersed and spherical in shape, with an average size of about 60 nm. It can be seen clearly that the silica-coated NPs have a core-shell structure, and the thickness of the silica shell is about 7 nm. Figure 5b shows the FT-IR spectrum of $NaYb_{0.98}F_4$:$Er_{0.02}$ NPs after silica-coating. The hydroxyl stretching vibration band of silanol group (Si-OH) appears in the region around 3436 cm^{-1}, corresponding to the stretching vibration of hydroxyl group. In addition, a strong transmission band attributed to the stretching vibration of Si-O bond can be seen at 1083 cm^{-1} in the spectra.

3.5. Synthesis of $NaYbF_4$:Er/Tm/Ho@SiO_2 multicolored UC NPs

Besides $NaYb_{0.98}F_4$:$Er_{0.02}$@SiO_2 NPs, NPs doped with other RE^{3+} ions are synthesized in the same way and their UC fluorescent properties have also been investigated. For $NaYb_{0.98}F_4$:$Er_{0.02}$ NPs, two green emissions at 520.5 and 540.5 nm, which can be assigned to the $^2H_{11/2}\rightarrow{}^4I_{15/2}$ and $^4S_{3/2}\rightarrow{}^4I_{15/2}$ transitions of Er^{3+}, and a red emission at 654.5 nm, which can be assigned to the $^4F_{9/2}\rightarrow{}^4I_{15/2}$ transition of Er^{3+}, were observed. Apparently, the UC fluorescence of the NPs appears orange in color (inset of Figure 7a) due to a combination of green and red emissions. The UC fluorescence of $NaYb_{0.98}F_4$:$Tm_{0.02}$ NPs appears pure blue in color (inset of Figure 7b) due to the two strong blue emissions at 450 and 475.5 nm, which were corresponding to the $^1D_2\rightarrow{}^3F_4$ and $^1G_4\rightarrow{}^3H_6$ transitions of Tm^{3+}, respectively. The $NaYb_{0.98}F_4$:$Ho_{0.02}$ NPs exhibit a green emission at 541 nm, resulting from the $^5S_2\rightarrow{}^5I_8$ transition of Ho^{3+}. Further, the NPs with multicolor emissions are achieved in a three-component doped system of $NaYb_{0.98}F_4$:Er/Tm/Ho after tuning. As presented in figure 7d-f, the silica-coated $NaYb_{0.98}F_4$:$Er_{0.01}$,$Tm_{0.01}$, $NaYb_{0.98}F_4$:$Tm_{0.01}$,$Ho_{0.01}$ and $NaYb_{0.98}F_4$:$Er_{0.01}$,$Ho_{0.01}$ NPs exhibit a pink, cyan and yellow emission, respectively, resulting from a dual emission process. Thus, a multicolor system of $NaYb_{0.98}F_4$:Er/Tm/Ho, which can emit orange, yellow, green, cyan, blue, and pink light depending on the doping concentration, is established. Their corresponding CIE (Commission Internationale de l'Eclairage 1931

chromaticity) coordinates are presented in Table S1 and plotted in Figure S2 (see Supporting Information).

3.6. Immunolabeling and fluorescent imaging of HeLa cells by using $NaYbF_4$:Er/Tm/Ho multicolored UC NPs

The immunolabeling and fluorescent imaging of HeLa cells by using $NaYbF_4$:Er/Tm/Ho multicolored UC NPs were conducted to investigate the potential applications of these multicolored UC NPs in bioimaging. In order to gain the biocompatibility, the UC NPs were first amino-functionalized by the hydrolysis of APTES via a typical Stöber method. Then, the amino-modified UC NPs were cross-linked with the rabbit anti-CEA8 antibody (Ab) by the aid of NHS and EDC. After the rabbit anti-CEA8 Ab conjugated UC NPs were incubated with live HeLa cells under the physiological conditions for 1 h, the immunoreaction between the rabbit anti-CEA8 Ab conjugated on the surface of the UC NPs and the CEA8 antigens expressed on HeLa cells membrane occurred, and the UC NPs were thus linked to the surface of the cells due to the antibody-antigen recognition. As a result, HeLa cells were fluorescently labeled by $NaYbF_4$:Er/Tm/Ho UC NPs. To verify the labeling of HeLa cells, the cells were imaged using an inverted fluorescence microscope equipped with a 980 nm NIR laser (Figure S1). It can be clearly seen in Figure 8 that the cells exhibit bright orange (Figure 8a), blue (Figure 8b), and green (Figure 8c) UC fluorescence on the surface of cells, respectively, which confirms that the rabbit anti-CEA8 Ab conjugated UC NPs are attached on the cell membrane with a good specificity. This fact indicates that the multicolored UC NPs with good biocompatibility recognize the targets on the cell membrane and the UC fluorescence is strong enough for the cell imaging (31, 36, 44-46).

To investigate the specific recognition and combination of this cell labeling, the amino-modified $NaYb_{0.98}F_4$:$Er_{0.02}$ UC NPs without any antibody linked were also incubated with live HeLa cells under the same physiological conditions as a negative control. Because there is no immunoreaction between the amino-modified UC NPs and the CEA8 antigen, the amino-modified UC NPs cannot specifically recognize the CEA8 antigens expressed on HeLa cells, and they fail to be combined with HeLa cells efficiently. As shown in Figure 9, only little orange fluorescence could be observed over the surface of the cells due to the non-specific binding between the UC NPs and the cells. However, the weak fluorescence from non-specific binding had little effect on cell imaging. Because the visible light emission of the $NaYbF_4$:Er/Tm/Ho UC NPs can be triggered by excitation using a NIR light and NIR light can penetrate tissue without the tissue damage, the UC NPs can find potential applications in in vivo and in vitro bioimaging.

4. Conclusions

In summary, Er^{3+}, Tm^{3+} and Ho^{3+} ions co-doped $NaYbF_4$ UC NPs were synthesized in the water-ethanol-oleic acid system via a two-phase solvothermal method. The NPs were in the size range of 15~30 nm with a strong UC fluorescent intensity. Synthesis parameters including reaction time and solvothermal temperature showed great influence on the size, phase structure and UC fluorescent intensity of the NPs. These results were related to the cubic-to-hexagonal phase transition. Silica coating of the NPs enabled water dispersibility. Co-doping of Er^{3+}, Tm^{3+} and Ho^{3+} ions in a single $NaYbF_4$ host resulted in multicolor emission, including orange, yellow, green, cyan, blue or pink color, depending on the doping concentration. After surface amino-functionalizing, the UC NPs were linked to the rabbit anti-CEA8 antibody and then used as the fluorescent biolabels for the immunolabeling and imaging of live HeLa cells. Compared with the controlled experiment, this immunolabeling of HeLa cells was specific. These $NaYbF_4$:Er/Tm/Ho UC NPs with multicolors are expected to find potential applications in in vivo and in vitro bioimaging and in multiplexed analysis.

Supplementary Material

Refer to Web version on PubMed Central for supplementary material.

Acknowledgments

We are grateful for the support from the National Science Foundation of China (Grant Nos 20875011, and 20725517) and the support from The Education Committee of Liaoning Province. CBM would like to acknowledge the financial support from US NSF, National Institutes of Health, DoD Congressionally Directed Medical Research Program, and Oklahoma Center for the Advancement of Science and Technology.

References and Notes

(1). Gao XH, Cui YY, Levenson RM, Chung LWK, Nie SM. Nat. Biotechnol 2004;22:969. [PubMed: 15258594]

(2). Goldman ER, Clapp AR, Anderson GP, Uyeda HT, Mauro JM, Medintz IL, Mattoussi H. Anal. Chem 2004;76:684. [PubMed: 14750863]

(3). Han MY, Gao XH, Su JZ, Nie SM. Nat. Biotechnol 2001;19:631. [PubMed: 11433273]

(4). Bruchez M, Moronne M, Gin P, Weiss S, Alivisatos AP. Science 1998;281:2013. [PubMed: 9748157]

(5). Liu JW, Lee JH, Lu Y. Anal. Chem 2007;79:4120. [PubMed: 17477504]

(6). Ma Q, Wang XY, Li YB, Shi YH, Su XG. Talanta 2007;72:1446. [PubMed: 19071782]

(7). Wu XY, Liu HJ, Liu JQ, Haley KN, Treadway JA, Larson JP, Ge NF, Peale F, Bruchez MP. Nat. Biotechnol 2003;21:41. [PubMed: 12459735]

(8). Ehlert O, Thomann R, Darbandi M, Nann T. ACS Nano 2008;2:120. [PubMed: 19206555]

(9). Heer S, Kömpe K, Güdel HU, Haase M. Adv. Mater 2004;16:2102.

(10). Zeng JH, Su J, Li ZH, Yan RX, Li YD. Adv. Mater 2005;17:2119.

(11). Wei Y, Lu FQ, Zhang XR, Chen DP. Matter. Lett 2007;61:1337.

(12). Wang XF, Xiao SG, Bu YY, Yang XL, Ding JW. J. Lumin 2009;129:325.

(13). Suyver JF, Grimm J, van Veen MK, Biner D, Krämer KW, Güdel HU. J. Lumin 2006;117:1.

(14). Auzel F. Chem. Rev 2004;104:139. [PubMed: 14719973]

(15). Yi GS, Chow GM. Chem. Mater 2007;19:341.

(16). Chen ZG, Chen HL, He H, Yu MX, Li FY, Zhang Q, Zhou ZG, Yi T, Huang CH. J. Am. Chem. Soc 2008;130:3023. [PubMed: 18278910]

(17). Wang X, Li YD. Chem. Commun 2007;28:2901.

(18). Wang F, Liu XG. J. Am. Chem. Soc 2008;130:5642. [PubMed: 18393419]

(19). Liu CH, Chen DP. J. Mater. Chem 2007;17:3875.

(20). Lu HC, Yi GS, Zhao SY, Chen DP, Guo LH, Cheng J. J. Mater. Chem 2004;14:1336.

(21). Zhang YW, Sun X, Si R, You LP, Yan CH. J. Am. Chem. Soc 2005;127:3260. [PubMed: 15755126]

(22). Du YP, Zhang YW, Yan ZG, Sun LD, Gao S, Yan CH. Chem. Asian J 2007;2:965. [PubMed: 17534994]

(23). Mai HX, Zhang YW, Sun LD, Yan CH. J. Phys. Chem. C 2007;111:13721.

(24). Mai HX, Zhang YW, Sun LD, Yan CH. J. Phys. Chem. C 2007;111:13730.

(25). Boyer JC, Cuccia LA, Capobianco JA. Nano Lett 2007;7:847. [PubMed: 17302461]

(26). Boyer JC, Vetrone F, Cuccia LA, Capobianco JA. J. Am. Chem. Soc 2006;128:7444. [PubMed: 16756290]

(27). Yi GS, Chow GM. Adv. Funct. Mater 2006;16:2324.

(28). Yi GS, Chow GM. J. Mater. Chem 2005;15:4460.

(29). Li CX, Quan ZW, Yang J, Yang PP, Lin J. Inorg. Chem 2007;46:6329. [PubMed: 17602610]

(30). Wang X, Zhuang J, Peng Q, Li YD. Inorg. Chem 2006;45:6661. [PubMed: 16903720]

(31). Wang F, Chatterjee DK, Li ZQ, Zhang Y, Fan XP, Wang MQ. Nanotechnology 2006;17:5786.

(32). Yi GS, Lu HC, Zhao SY, Ge Y, Yang WJ, Chen DP, Guo LH. Nano Lett 2004;4:2191.

(33). Wei Y, Lu FQ, Zhang XR, Chen DP. J. Alloy. Compd 2007;427:333.

(34). Wang X, Zhuang J, Peng Q, Li YD. Nature 2005;437:121. [PubMed: 16136139]
(35). Liang X, Wang X, Zhuang J, Peng Q, Li YD. Adv. Funct. Mater 2007;17:2757.
(36). Kumar R, Nyk M, Ohulchanskyy TY, Flask CA, Prasad PN. Adv. Funct. Mater 2009;19:853.
(37). Wang LY, Yan RX, Huo ZY, Wang L, Zeng JH, Bao J, Wang X, Peng Q, Li YD. Angew. Chem. Int. Ed 2005;44:6054.
(38). Jiang S, Zhang Y, Lim KM, Sim EKW, Ye L. Nanotechnology 2009;20:155101. [PubMed: 19420539]
(39). Wang M, Liu JL, Zhang YX, Hou W, Wu XL, Xu SK. Mater. Lett 2009;63:325.
(40). Wei Y, Lu FQ, Zhang XR, Chen DP. Chem. Mater 2006;18:5733.
(41). Thoma RE, Insley H, Hebert GM. Inorg. Chem 1966;5:1222.
(42). Mai HX, Zhang YW, Si R, Yan ZG, Sun LD, You LP, Yan CH. J. Am. Chem. Soc 2006;128:6426. [PubMed: 16683808]
(43). Liang LF, Wu H, Hu HL, Wu MM, Su Q. J. Alloy. Compd 2004;368:94.
(44). Nyk M, Kumar R, Ohulchanskyy TY, Bergey EJ, Prasad PN. Nano Lett 2008;8:3834. [PubMed: 18928324]
(45). Chatterjee DK, Rufaihah AJ, Zhang Y. Biomaterials 2008;29:937. [PubMed: 18061257]
(46). Jalil RA, Zhang Y. Biomaterials 2008;29:4122. [PubMed: 18675453]

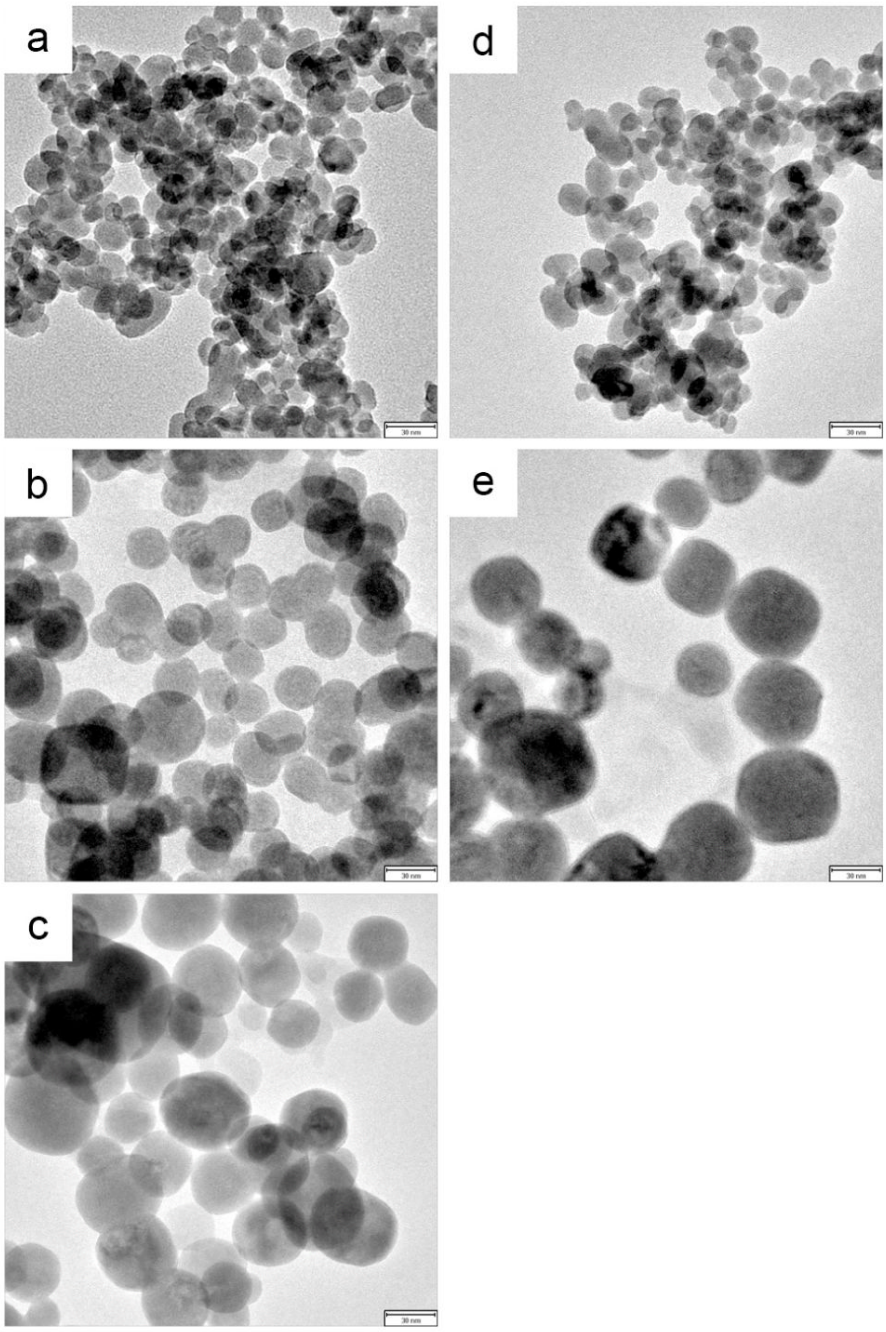

Figure 1.

TEM images of $NaYb_{0.98}F_4:Er_{0.02}$ NPs synthesized at varying reaction time and temperature: 150 °C for 2 h (a), 150 °C for 8 h (b), 150 °C for 24 h (c), 100 °C for 8 h (d), and 200 °C for 8 h (e). The scale bar in the inset corresponds to 30 nm.

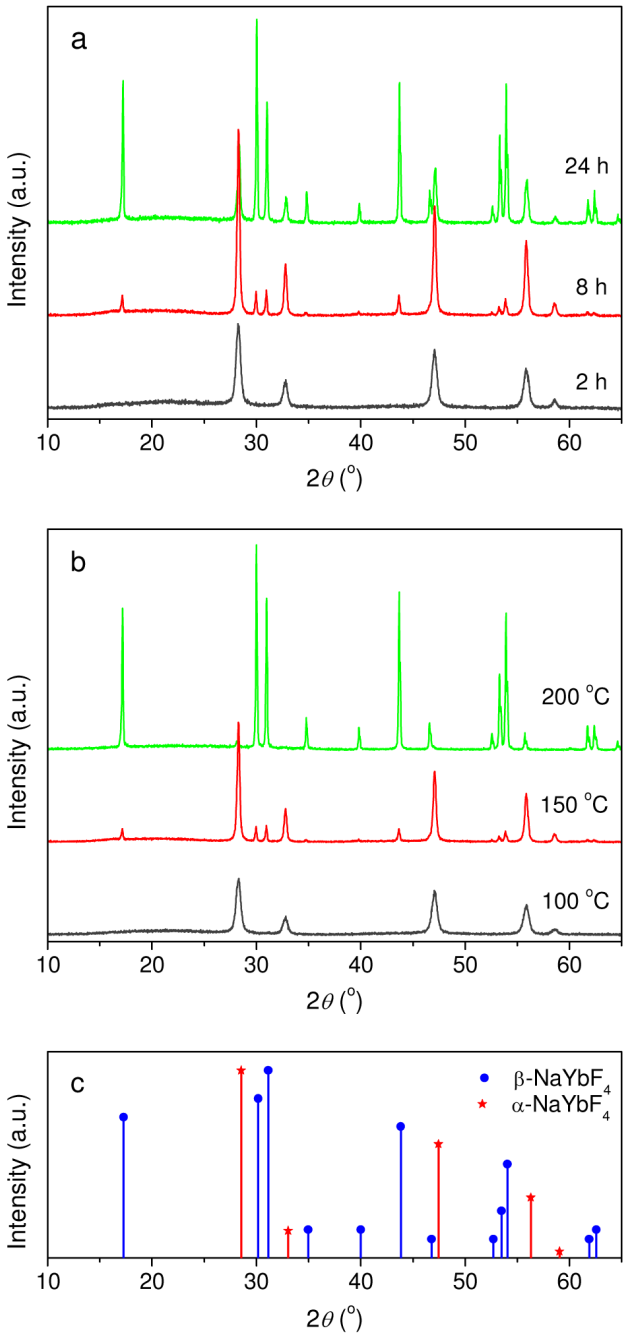

Figure 2.

XRD patterns of the $NaYb_{0.98}F_4$:$Er_{0.02}$ NPs synthesized at different reaction time with a constant reaction temperature of 150 °C (a), and at different temperature for constant reaction time of 8 h (b) as well as calculated line pattern for cubic α-phase $NaYbF_4$ and hexagonal β-phase $NaYbF_4$ (c).

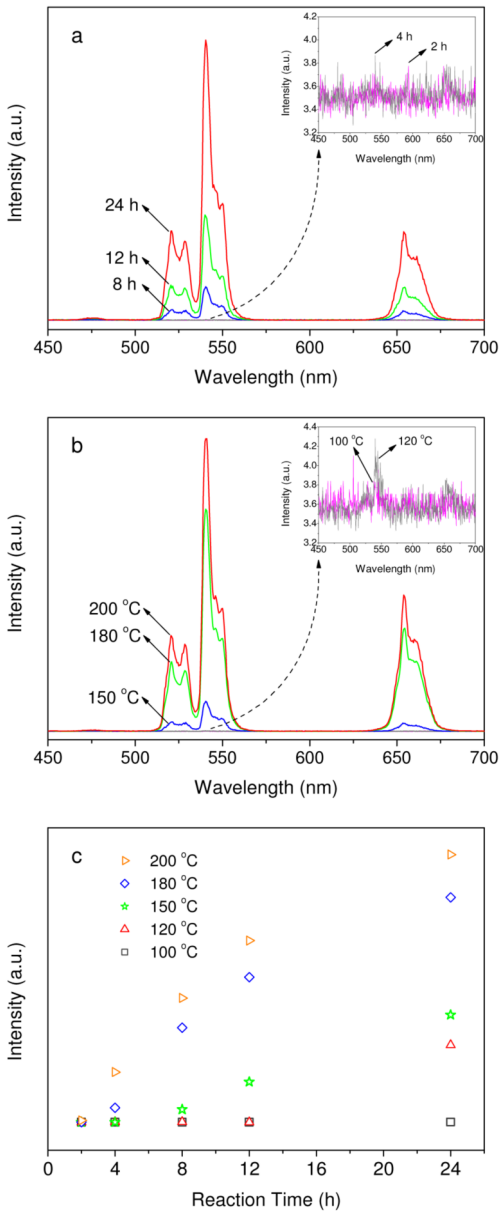

Figure 3.

UC fluorescence spectra of the powder $NaYb_{0.98}F_4:Er_{0.02}$ NPs synthesized at different reaction times with a constant reaction temperature of 150 °C (a), at different temperatures for a constant reaction time of 8 h (b) and UC fluorescence intensity (emission at 541 nm) at different reaction times (2~24 h) and temperatures (100~200 °C) (c). The excited power is 64 mW and the emission slit is 2.5 nm.

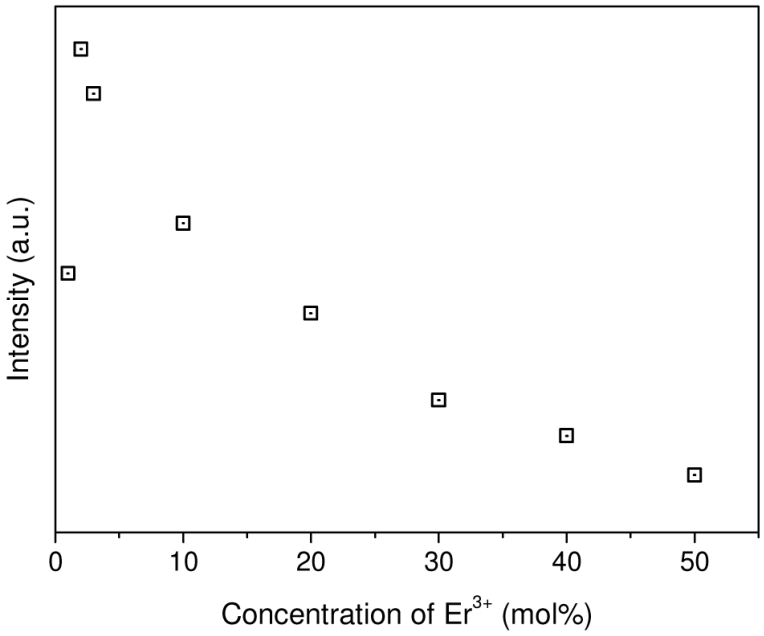

Figure 4.
Variation of UC intensity of $NaYbF_4$:Er NPs with different dopant concentrations of Er^{3+}. The excitation power of 980 nm laser is 64 mW.

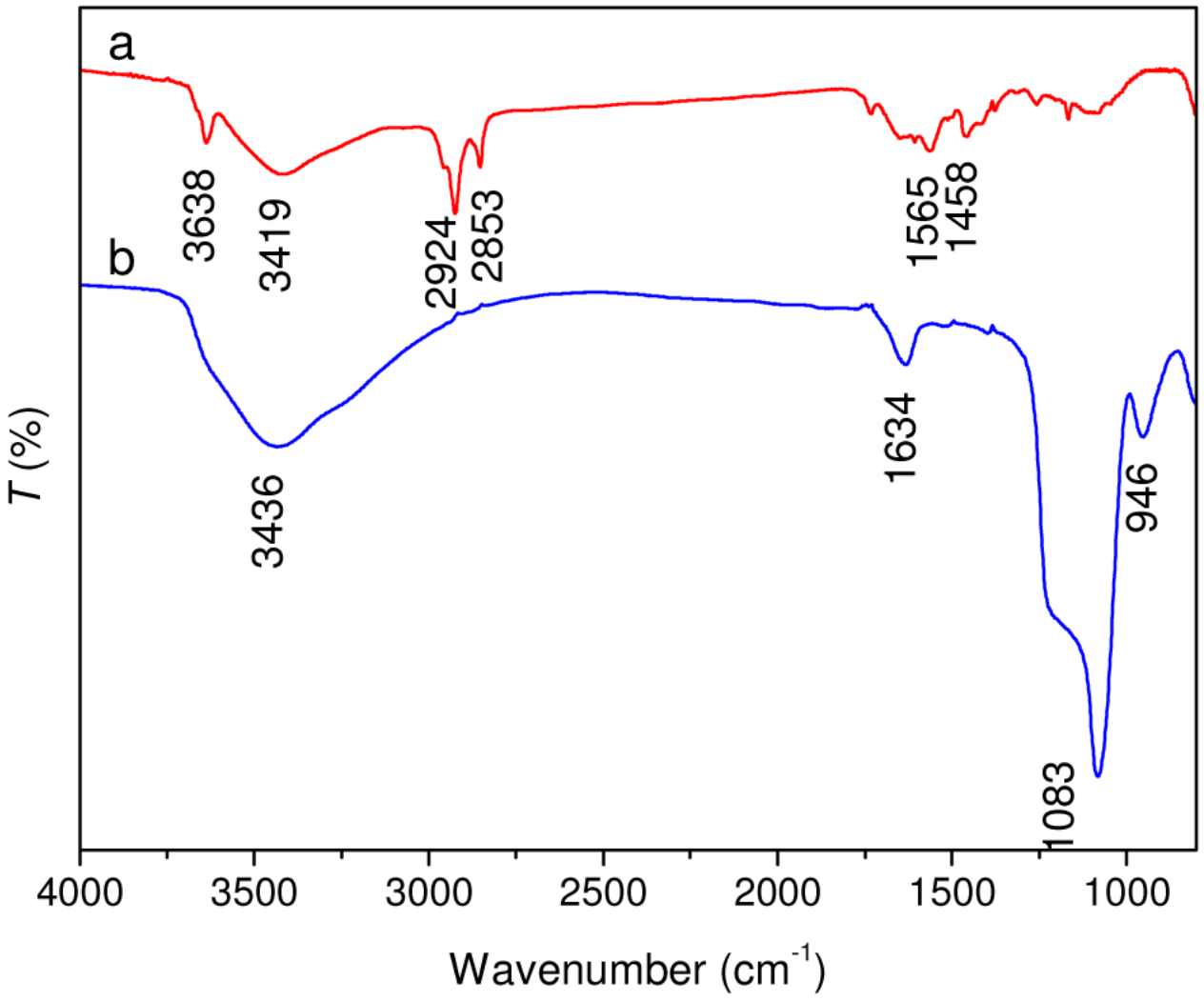

Figure 5.
FT-IR spectra of $NaYb_{0.98}F_4:Er_{0.02}$ (a) and $NaYb_{0.98}F_4:Er_{0.02}@SiO_2$ NPs (b).

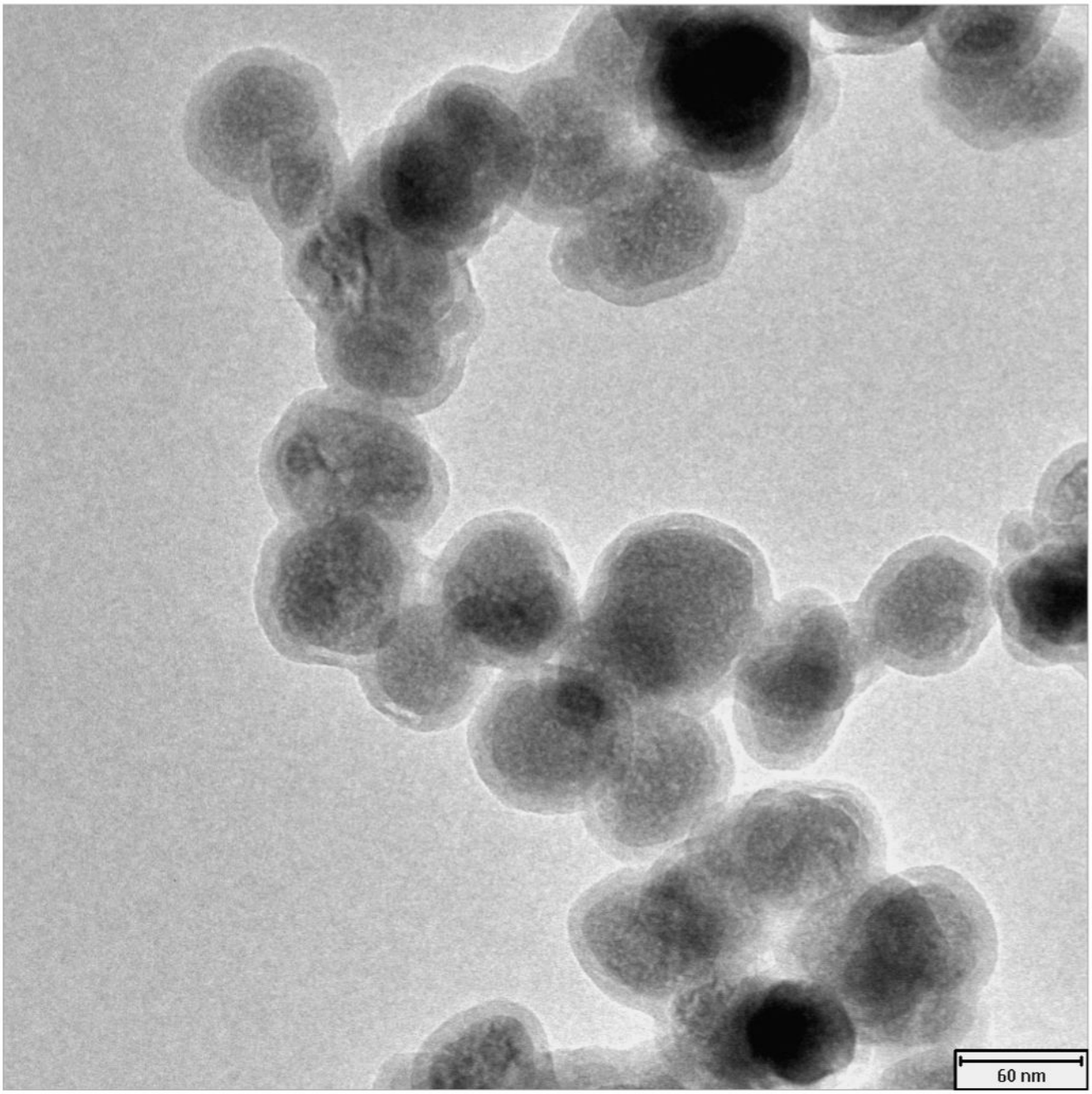

Figure 6.
TEM images of silica-coated $NaYb_{0.98}F_4:Er_{0.02}$ NPs. The scale bar in the inset corresponds to 60 nm.

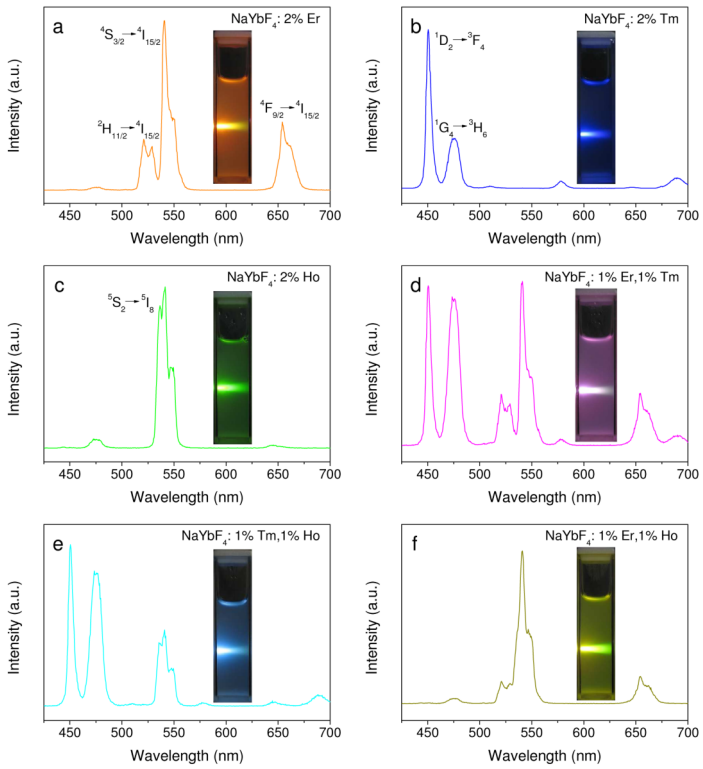

Figure7.

UC fluorescence spectra of 1 wt% colloidal solutions of $NaYb_{0.98}F_4$:$RE_{0.02}$@SiO_2 NPs in water excited with a 980 nm laser: (a) $NaYb_{0.98}F_4$:$Er_{0.02}$@SiO_2, (b) $NaYb_{0.98}F_4$:$Tm_{0.02}$@SiO_2, (c) $NaYb_{0.98}F_4$:$Ho_{0.02}$@SiO_2, (d) $NaYb_{0.98}F_4$:$Er_{0.01}$,$Tm_{0.01}$@SiO_2, (e) $NaYb_{0.98}F_4$:$Tm_{0.01}$,$Ho_{0.01}$@SiO_2, and (f) $NaYb_{0.98}F_4$:$Er_{0.01}$,$Ho_{0.01}$@SiO_2. Insets are the photographs of 1 wt% colloidal solutions of corresponding NPs in water, excited with a 980 nm laser.

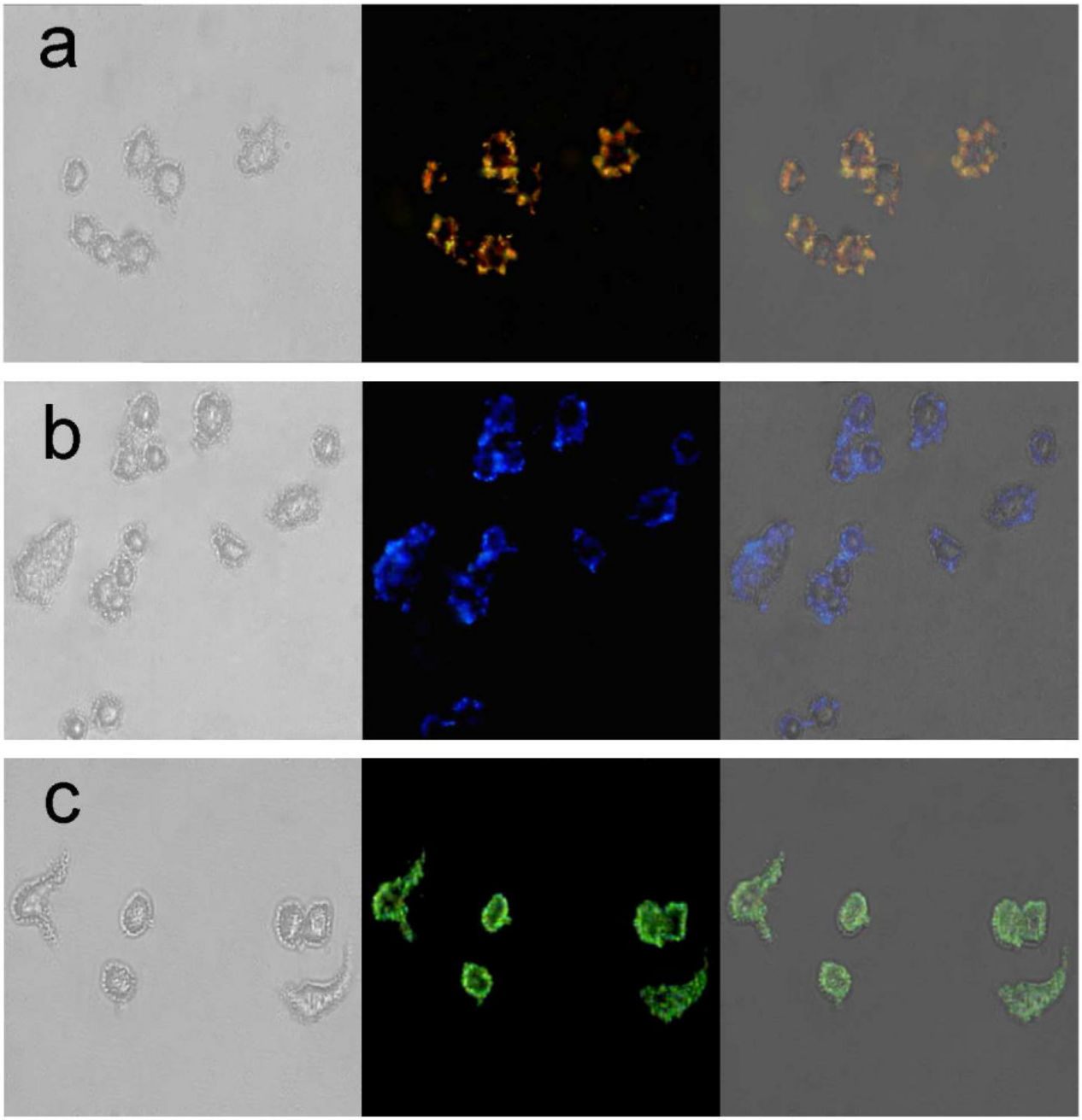

Figure 8.

Fluorescence imaging of HeLa cells after incubated with rabbit anti-CEA8 Ab conjugated (a) $NaYb_{0.98}F_4:Er_{0.02}$, (b) $NaYb_{0.98}F_4:Tm_{0.02}$, and (c) $NaYb_{0.98}F_4:Ho_{0.02}$ UC NPs for 1 h under a NIR irradiation (980 nm). Left rows are images in bright field, the middle rows are fluorescent images in dark field, and right rows are overlays of the left and central rows.

Figure 9.
Fluorescence imaging of HeLa cells after incubated with amino-functionalized $NaYb_{0.98}F_4$:$Er_{0.02}$ UC NPs for 1 h under a NIR irradiation (980 nm). Left rows are images in bright field, the middle rows are fluorescent images in dark field, and right rows are overlays of the left and central rows.